

CrystEngComm

Accepted Manuscript



This is an *Accepted Manuscript*, which has been through the Royal Society of Chemistry peer review process and has been accepted for publication.

Accepted Manuscripts are published online shortly after acceptance, before technical editing, formatting and proof reading. Using this free service, authors can make their results available to the community, in citable form, before we publish the edited article. We will replace this *Accepted Manuscript* with the edited and formatted *Advance Article* as soon as it is available.

You can find more information about *Accepted Manuscripts* in the [Information for Authors](#).

Please note that technical editing may introduce minor changes to the text and/or graphics, which may alter content. The journal's standard [Terms & Conditions](#) and the [Ethical guidelines](#) still apply. In no event shall the Royal Society of Chemistry be held responsible for any errors or omissions in this *Accepted Manuscript* or any consequences arising from the use of any information it contains.

Cite this: DOI: 10.1039/c0xx00000x

www.rsc.org/xxxxxx

ARTICLE TYPE

Well-Controlled Synthesis of Wurtzite-Type $\text{Cu}_2\text{ZnSnS}_4$ Nanoparticles Using Multiple Sulfur Sources via a Two-Step Heating Process

Hiroyasu Nishi,^{*‡^a} Takahito Nagano,^a Tatsuya Kameyama,^a Susumu Kuwabata,^b and Tsukasa Torimoto^{*^a}

Received (in XXX, XXX) Xth XXXXXXXXX 20XX, Accepted Xth XXXXXXXXX 20XX

DOI: 10.1039/b000000x

Wurtzite-type copper zinc tin sulfide ($\text{Cu}_2\text{ZnSnS}_4$) nanoparticles were prepared in dodecanethiol (DDT) solutions by reacting corresponding metal acetates with a mixture of sulfur compounds with different reactivities, elemental sulfur (S) and dibutylthiourea (DBTU), via a two-step heat treatment. Initial heating at 200 °C enabled the nucleation of metal sulfide nanoparticles comprised of two crystal phases, and subsequent heat treatment at 240 °C resulted in the formation of $\text{Cu}_2\text{ZnSnS}_4$ nanoparticles with a wurtzite-type crystal structure. The resulting particles had rod shapes with a stoichiometric composition, the size and shape of which could be controlled by changing both the reaction time and the molar ratio of S and DBTU used in a sulfur precursor. In contrast, spherical $\text{Cu}_2\text{ZnSnS}_4$ nanoparticles with a kesterite-type crystal structure were produced by reaction with pure S as a precursor. The electronic energy levels of the conduction band and valence band edges were determined for wurtzite-type $\text{Cu}_2\text{ZnSnS}_4$ nanoparticles by photoelectrochemical measurement, the individual levels being comparable to those of kesterite-type ones. The light-electricity conversion efficiency varied remarkably depending on the kind of crystal structure: wurtzite-type $\text{Cu}_2\text{ZnSnS}_4$ particles exhibited an efficiency superior to that of the particles with a kesterite crystal structure.

1. Introduction

A semiconductor of copper zinc tin sulfide ($\text{Cu}_2\text{ZnSnS}_4$) has been regarded as an attractive candidate for a light-absorbing material in next-generation photovoltaic devices¹⁻⁵ because all of the elements constituting the semiconductor are earth-abundant elements with little toxicity unlike conventional metal chalcogenide semiconductors such as cadmium chalcogenide,⁶ lead chalcogenide,⁷ and copper indium gallium selenide (CIGS),^{8,9} which have been used in efficient compound semiconductor solar cells showing an efficiency of ca. 20%. Due to the attractive optical properties of $\text{Cu}_2\text{ZnSnS}_4$, such as a proper band gap (~1.5 eV) for solar cell application and high absorption coefficient in the wavelength region from visible to near-IR light, intensive research works have been carried out to fabricate thin-film solar cells with a $\text{Cu}_2\text{ZnSnS}_4$ layer as a light absorbing material, and the solar energy conversion efficiency has recently reached 12.6%,³ approaching the efficiency of conventional amorphous silicon or compound semiconductor-based solar cells.

In order to prepare a $\text{Cu}_2\text{ZnSnS}_4$ thin film at a low cost, much attention has been paid to $\text{Cu}_2\text{ZnSnS}_4$ nanoparticles synthesized via solution-based approaches. Aqueous or organic suspensions of $\text{Cu}_2\text{ZnSnS}_4$ nanoparticles can be used as nanoparticle ink, and then sintering $\text{Cu}_2\text{ZnSnS}_4$ nanoparticle films deposited on a substrate under appropriate conditions can produce a high-quality

bulk $\text{Cu}_2\text{ZnSnS}_4$ film. Such a technique pioneered by Agrawal *et al.* in 2009¹⁰ has reported to yield a thin $\text{Cu}_2\text{ZnSnS}_4$ film easily and inexpensively in comparison with other techniques such as spray pyrolysis, electron beam evaporation, sputtering, and chemical deposition. It has also been reported that thin-film solar cells composed of $\text{Cu}_2\text{ZnSn}(\text{S},\text{Se})_4$, fabricated by sintering $\text{Cu}_2\text{ZnSnS}_4$ nanoparticles in selenium vapor,¹¹ exhibited relatively high conversion efficiency of 7.2%. Furthermore, $\text{Cu}_2\text{ZnSnS}_4$ nanoparticles with diameters of less than ca. 5 nm have been reported by Aydil *et al.* and Liu *et al.*^{12,13} to exhibit size-dependent absorption properties of $\text{Cu}_2\text{ZnSnS}_4$ nanoparticles due to the quantum size effect, and they have been of great interest as a light-absorbing material in highly efficient quantum dot solar cells.¹⁴ We have recently clarified that size-quantized $\text{Cu}_2\text{ZnSnS}_4$ nanoparticles had a tunable electronic energy structure depending on their size¹⁵ and that their light-electricity conversion efficiency was greatly varied by the chemical composition of particles.¹⁶

The thermodynamically stable crystal structure of $\text{Cu}_2\text{ZnSnS}_4$ is usually kesterite, which is derived from a zinc-blend lattice with a tetragonal crystal cell. However, $\text{Cu}_2\text{ZnSnS}_4$ nanoparticles with a metastable wurtzite-derived structure have been reported in recent years.¹⁷⁻²⁴ The wurtzite-type $\text{Cu}_2\text{ZnSnS}_4$ could be exclusively seen in the form of nanoparticles that had unique shapes derived from the wurtzite-type structure of a hexagonal crystal lattice. Most of the wurtzite-type $\text{Cu}_2\text{ZnSnS}_4$ nanoparticles were

synthesized by the hot-injection method,^{17,18,23,24} while some researchers used one-pot heating synthesis.¹⁹⁻²² Peng *et al.* first synthesized wurtzite-type $\text{Cu}_2\text{ZnSnS}_4$ by hot-injection of metal chlorides dissolved in 1-dodecanethiol (DDT) into a mixed solvent of DDT, oleylamine (OLA) and/or oleic acid (OAc) at 240 °C.¹⁷ Ryan *et al.* reported high-quality and monodispersed wurtzite-type $\text{Cu}_2\text{ZnSnS}_4$ nanorods prepared by injection of DDT and *tert*-dodecyl mercaptan (*t*-DDT) into 1-otadecene (ODE) containing copper(II) acetylacetonate, zinc(II) acetate, tin(IV) acetate, and trioctylphosphine oxide (TOPO).¹⁸ Since wurtzite-type $\text{Cu}_2\text{ZnSnS}_4$ nanoparticles were reported to have a higher carrier concentration and lower resistivity than those of kesterite-type ones,¹⁹ they have attracted attention as a novel light-absorbing material for photovoltaic applications. Although diverse techniques for the syntheses of wurtzite-type nanoparticles, in which various reagents were used without noting their functions, have been reported, the reaction conditions have not been optimized despite the considerable interest shown in characteristics of wurtzite-type $\text{Cu}_2\text{ZnSnS}_4$ nanoparticles. Furthermore, there have been only a few reports on semiconductor photoelectrodes fabricated with wurtzite-type $\text{Cu}_2\text{ZnSnS}_4$ nanoparticles.

Several researchers have recently demonstrated that wurtzite-type $\text{Cu}_2\text{ZnSnS}_4$ grew from a djurleite ($\text{Cu}_{1.94}\text{S}$) nanoparticle as the nucleus.^{19-21,23} Vela *et al.* and Jiang *et al.* showed that controlling reactivity of metal precursors with a sulfur source to generate a djurleite nucleus is of great importance for the subsequent crystal growth of wurtzite-type $\text{Cu}_2\text{ZnSnS}_4$ nanoparticles.^{23,24} However, a method for synthesis in which the nucleation process can be clearly separated from the crystal growth processes has not been established. Thus, selective preparation of wurtzite-type $\text{Cu}_2\text{ZnSnS}_4$ nanoparticles is still a challenging issue. Herein, we propose a new approach to synthesize wurtzite-type $\text{Cu}_2\text{ZnSnS}_4$ nanoparticles using two different sulfur sources, elemental sulfur (S) and 1,3-dibutylthiourea (DBTU),²⁵ via a two-step heating process, in which the difference in reactivity of sulfur precursors with metal ions enables stable nucleus formation of a djurleite structure followed by crystal growth of wurtzite-type $\text{Cu}_2\text{ZnSnS}_4$ nanoparticles. The photoelectrochemical properties of wurtzite $\text{Cu}_2\text{ZnSnS}_4$ particles were investigated by immobilizing the thus-obtained particles on indium tin oxide (ITO) electrodes.

2. Experimental

2.1 Materials

Chemicals of copper(II) acetate ($\text{Cu}(\text{CH}_3\text{COO})_2$), zinc(II) acetate ($\text{Zn}(\text{CH}_3\text{COO})_2$), 1-dodecanethiol (DDT), and 1,3-dibutylthiourea (DBTU) were commercially available from Wako Pure Chemical Industries. Tin(IV) acetate ($\text{Sn}(\text{CH}_3\text{COO})_4$) was obtained from Aldrich. Europium(III) nitrate ($\text{Eu}(\text{NO}_3)_3$) hexahydrate and sulfur (S) were purchased from Kishida Chemical. All reagents were used as received. Aqueous solutions were prepared with water purified by a Millipore Milli-Q system.

2.2 Synthesis of wurtzite- and kesterite-type $\text{Cu}_2\text{ZnSnS}_4$ nanoparticles

A two-step heating process was adopted for the synthesis of wurtzite-type $\text{Cu}_2\text{ZnSnS}_4$ nanoparticles with the use of a mixture of S and DBTU as a sulfur precursor, a typical procedure of which is described below. Powders of $\text{Cu}(\text{CH}_3\text{COO})_2$ (0.10 mmol), $\text{Zn}(\text{CH}_3\text{COO})_2$ (0.050 mmol), and $\text{Sn}(\text{CH}_3\text{COO})_4$ (0.050 mmol) were dispersed in DDT (3.0 cm³). The suspension was heated at 200 °C for ca. 5 min with vigorous stirring in an N₂ atmosphere to yield a homogeneous transparent solution. To the solution, 0.30-cm³ DDT solution containing S (0.10 mmol) and DBTU (0.10 mmol) was quickly added, followed by stirring for 30 min at 200 °C. Then the reaction temperature was quickly raised to 240 °C and the solution was further stirred for 0-180 min. After cooling down to room temperature, the reaction mixture was subjected to centrifugation at 4000 rpm for 5 min. The resulting precipitates were washed with ethanol several times and dried under vacuum. The precipitates were again dissolved in hexane (2.0 cm³), followed by the removal of large precipitates by filtration through a syringe filter (pore size: 1.2 μm) before use. Kesterite-type $\text{Cu}_2\text{ZnSnS}_4$ nanoparticles could be prepared by a similar method except for the addition of pure elemental S (0.20 mol) as a sulfur precursor. Reaction conditions, including the molar ratio of S and DBTU used as a sulfur precursor, reaction temperature at each heating process, and reaction time, were varied to investigate the influence of these parameters on the morphology of $\text{Cu}_2\text{ZnSnS}_4$ nanoparticles and their crystal structure.

2.3 Characterization of nanoparticles

The chemical composition of particles was determined by X-ray fluorescence (XRF) spectroscopy (Rigaku, EDXL-300) or energy dispersive X-ray (EDX) analysis using a Hitachi SU-1500 scanning electron microscope equipped with an EDX analyzer (Horiba, EMAX ENERGY EX-250). The shape and size distribution of the obtained particles were observed by a Hitachi H7650 transmission electron microscope (TEM) with an acceleration voltage at 100 kV. Samples for TEM measurements were prepared by dropping a hexane solution containing the particles onto a carbon-coated copper grid, followed by drying under reduced pressure. Average length and width of the particles were determined by measuring the dimensions of at least 100 particles in the TEM images. A Rigaku Smart Lab powder X-ray diffraction (XRD) instrument equipped with an X-ray tube (Cu K α radiation: $\lambda = 1.54059 \text{ \AA}$, 40 kV, 30 mA) was used for analyzing the crystal structure of particles, with measurements being carried out for samples put on a low-background silicon sample holder. Absorption spectra of particles in hexane were obtained by using an Agilent Technology 8453 UV-visible spectrophotometer.

2.4 Photoelectrochemical measurements

$\text{Cu}_2\text{ZnSnS}_4$ nanoparticles were immobilized on ITO-coated glass electrodes for photoelectrochemical measurements. A hexane solution of the wurtzite-type $\text{Cu}_2\text{ZnSnS}_4$ nanoparticles was spin-coated onto an ITO electrode at 2000 rpm for 20 s. To immobilize the particles on the ITO, the electrode was heated at 250 °C for 5 min under reduced pressure. The absorbance of thus-obtained particle films was ca. 0.08 at 400 nm. The photoelectrochemical properties of the nanoparticle-immobilized

ITO electrodes were measured in an aqueous solution containing $0.20 \text{ mol dm}^{-3} \text{ Eu}(\text{NO}_3)_3$ ($\text{pH} = 2.3$) as an electron acceptor. The potential was determined against an Ag/AgCl (sat. KCl) reference electrode. A Pt wire was used as a counter electrode. The photocurrent was detected with a Hokuto Denko HAB-151A potentiostat. Light irradiation ($\lambda > 350 \text{ nm}$) to the electrode was carried out by passing light from a 300 W Xe lamp (USHIO X300) through a UV cut-off filter and a light chopper. The light intensity of the irradiation was ca. 0.9 W cm^{-2} at the electrode surface. Action spectra of the photocurrent were measured by irradiation of monochromatic light, which was obtained by passing light through a JASCO CT-10 monochromator. The incident photon-to-current efficiency (IPCE) was calculated by dividing the number of electrons detected in the photocurrent by that of incident photons.

3. Results and Discussion

3.1 Synthesis of wurtzite-type $\text{Cu}_2\text{ZnSnS}_4$ nanoparticles via a two-step heating process

It is well known that thiol compounds potentially act as a sulfur source for the preparation of metal sulfide particles: metal thiolate complexes, formed by the reaction of metal ions with thiols, can be decomposed via C-S bond cleavage at a high temperature,²⁶ allowing the formation of metal sulfide nanoparticles even without addition of sulfur sources such as elemental S. Therefore, we first investigated the reactivity of metal acetates with DDT. Powders of metal acetates were pre-heated in DDT in an N_2 atmosphere to obtain a homogeneous solution containing metal thiolates. Mixture powders of $\text{Cu}(\text{CH}_3\text{COO})_2$ (0.10 mmol), $\text{Zn}(\text{CH}_3\text{COO})_2$ (0.050 mmol), and $\text{Sn}(\text{CH}_3\text{COO})_4$ (0.050 mmol) were not completely dissolved in DDT (3.0 cm^3) at a temperature below ca. $120 \text{ }^\circ\text{C}$, but the solution became transparent by heat treatment at $150\text{--}200 \text{ }^\circ\text{C}$ for less than 5 min. On the other hand, heating the solution at a temperature higher than $240 \text{ }^\circ\text{C}$ produced dark brown precipitates within several minutes. Thus-obtained precipitates could not be dissolved in organic solvents such as hexane, toluene, and chloroform. TEM measurement (Fig. S1) revealed that the precipitates obtained by heat treatment at $240 \text{ }^\circ\text{C}$ for 60 min were composed of relatively large octahedron-like particles with diagonal lengths of $20\text{--}40 \text{ nm}$ as a result of thermal decomposition of metal thiolates. The particles had the chemical composition of $\text{Cu} : \text{Zn} : \text{Sn} = 0.86 : 0.07 : 0.07$, indicating that metal sulfides produced by decomposition of metal thiolates at $240 \text{ }^\circ\text{C}$ were not $\text{Cu}_2\text{ZnSnS}_4$ but mainly contained Cu as a metal species. Since the thermal decomposition may proceed gradually according to decomposition kinetics, it is thought that a small number of nuclei are generated in early stage of the reaction and crystal growth occurs simultaneously with the nucleation, resulting in formation of relatively large nanoparticles with a wide size distribution. In addition, a Cu precursor tends to form metal sulfide more easily than Zn and Sn ones.²³ Therefore, we used temperatures ranging from 150 to $200 \text{ }^\circ\text{C}$ for preparation of a metal acetate precursor solution without formation of undesired metal sulfides.

As the first heating process in $\text{Cu}_2\text{ZnSnS}_4$ preparation, a 0.30 cm^3 portion of DDT solution containing two different sulfur

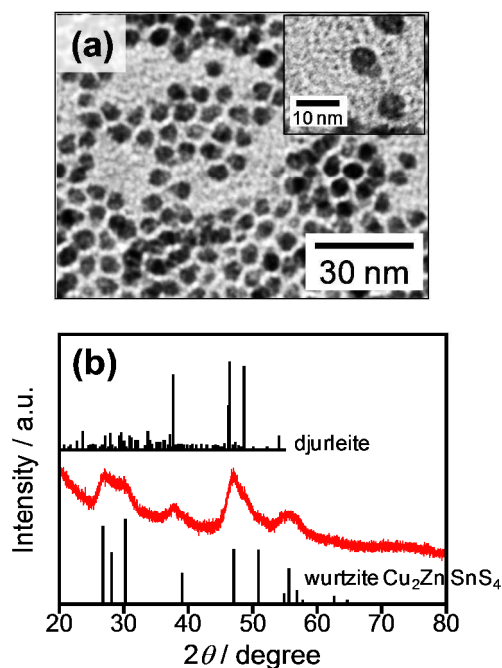


Fig. 1 TEM image (a) and XRD pattern (b) of nanoparticles obtained by injection of S and DBTU (S : DBTU = 50 : 50) into the precursor solution at $200 \text{ }^\circ\text{C}$ and stirring for 30 min (first heating process). Reference XRD pattern of djurleite (PDF card: #00-034-0660) and simulated pattern of wurtzite-type $\text{Cu}_2\text{ZnSnS}_4$ shown in ref. 17 are also shown.

sources, S (0.10 mmol) and DBTU (0.10 mmol), was injected into the metal thiolate precursor solution at $200 \text{ }^\circ\text{C}$, followed by stirring for 30 min. Fig. 1a shows representative TEM image of the thus-obtained nanoparticles. Mushroom-like polyagonal nanoparticles could be observed in the images, which consisted of at least two parts with different contrast, and the average sizes of the nanoparticles were ca. 7 nm in length and ca. 5 nm in width. The chemical composition of whole particles was determined to be $\text{Cu} : \text{Zn} : \text{Sn} = 0.79 : 0.13 : 0.08$. XRD patterns of the particles (Fig. 1b) revealed that the particles contained at least two crystal phases. Main peaks could be assigned to wurtzite phase of $\text{Cu}_2\text{ZnSnS}_4$, while a small peak at 38° could be assigned to the (842) plane of a djurleite crystal with a monoclinic structure. Since wurtzite-type $\text{Cu}_2\text{ZnSnS}_4$ nanoparticles have been reported to grow from the nuclei of djurleite ($\text{Cu}_{1.94}\text{S}$) nanoparticles,^{19-21,23} it is reasonable to assign the diffraction pattern to the mixture of djurleite ($\text{Cu}_{1.94}\text{S}$) and wurtzite $\text{Cu}_2\text{ZnSnS}_4$ crystal phases. Prolongation of the reaction time from 30 to 180 min still resulted in the formation of polyagonal particles composed of a mixture of crystal phases but not pure wurtzite $\text{Cu}_2\text{ZnSnS}_4$ (Fig. S2).

In contrast, increase in the reaction temperature, represented as the second heating process in the present study, resulted in conversion of the mixed crystal phases of metal sulfide particles into pure wurtzite phase. Just after the reaction of metal acetates with a mixture of S and DBTU in DDT at $200 \text{ }^\circ\text{C}$ for 30 min, heating the reaction solution at a higher temperature of 240 or $270 \text{ }^\circ\text{C}$ for 30 min resulted in the formation of nanoparticles with rod-like shapes as shown in Fig. 2a and b, the average lengths and widths being 9.3 and 5.7 nm for $240 \text{ }^\circ\text{C}$ and 10.7 and 7.0 nm for

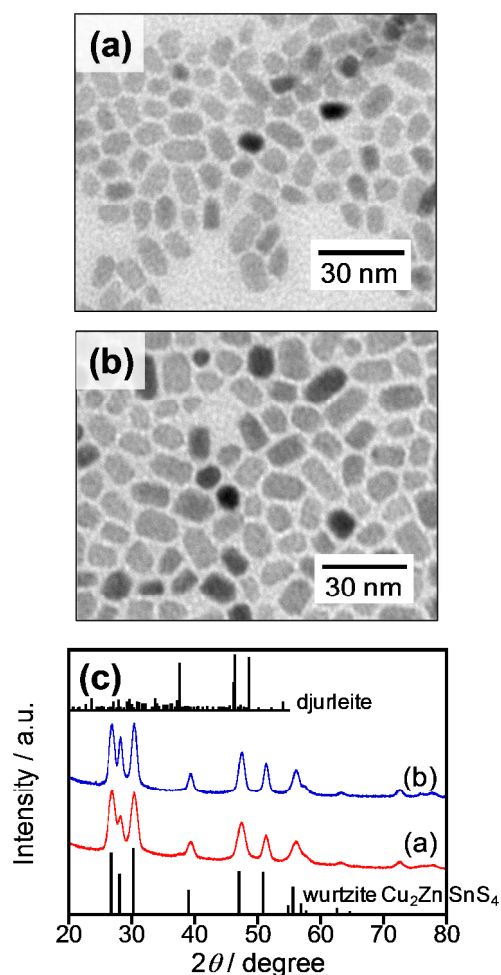


Fig. 2 (a,b) TEM images of nanoparticles obtained by heating at 240 °C (a) and 270 °C (b) for 30 min in the second heating process. The solution used was prepared by heating at 200 °C for 30 min in the first heating process after the injection of a sulfur precursor (S : DBTU = 50 : 50). (c) Corresponding XRD patterns for the nanoparticles shown in panels a and b. Reference pattern of djurleite (PDF card: #00-034-0660) and simulated pattern of wurtzite-type Cu₂ZnSnS₄ shown in ref. 17 are also shown.

270 °C, respectively. The chemical compositions of particles obtained at 240 °C and 270 °C were Cu : Zn : Sn = 0.57 : 0.20 : 0.23 and 0.48 : 0.22 : 0.28, respectively, being close to stoichiometric chemical composition of Cu₂ZnSnS₄ (Cu : Zn : Sn = 0.50 : 0.25 : 0.25). These results indicated that Zn and Sn ions were sufficiently incorporated into the particles in the second heating process. Fig. 2c shows XRD patterns of the resulting particles. The diffraction peaks observed for each kind of particles could be definitely assigned to the wurtzite Cu₂ZnSnS₄ crystal phase, while there was no secondary crystal phase, such as djurleite Cu_{1.94}S or other metal sulfides. In the case of nucleation

Consequently, wurtzite-type Cu₂ZnSnS₄ nanoparticles were successfully obtained via a two-step heating process (200 °C for 30 min followed by 240 or 270 °C for 30 min) with the second step requiring a reaction temperature higher than 240 °C for the formation of stoichiometric wurtzite-type Cu₂ZnSnS₄ nanoparticles. We could assume in the present study that the first

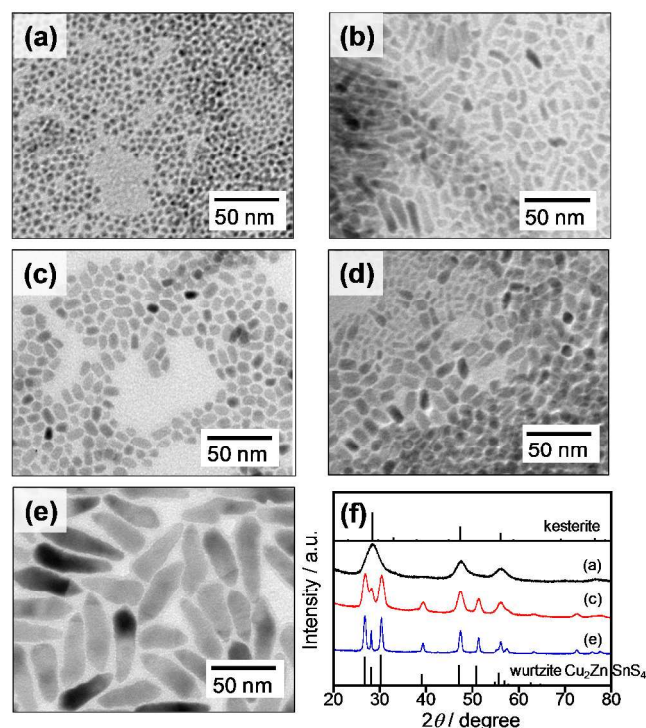


Fig. 3 (a-e) TEM images of nanoparticles obtained by reactions using various ratios of S and DBTU. The ratios of S : DBTU were 100 : 0 (a), 75 : 25 (b), 50 : 50 (c), 25 : 75 (d), and 0 : 100 (e). (f) Corresponding XRD patterns for the nanoparticles shown in panels a, c, and e. Reference pattern of kesterite Cu₂ZnSnS₄ (PDF card: #01-075-4122) and simulated pattern of wurtzite-type Cu₂ZnSnS₄ shown in ref. 17 are also shown.

heating process at 200 °C for 30 min after the addition of sulfur sources of S and DBTU was the "nucleation process" giving mushroom-like nanoparticles as shown in Fig. 1 and that the following heating process at 240 or 270 °C was the "crystal growth process" of wurtzite Cu₂ZnSnS₄ nanoparticles. It should be noted that the decrease in the nucleation temperature to 150 °C from 200 °C hardly changed the morphology of the resulting particles: When the heating in nucleation process was carried out at 150 °C for 30 min followed by the crystal growth process at 240 °C for 30 min, pure wurtzite Cu₂ZnSnS₄ nanoparticles were produced as shown in Fig. S3 with average length and width of 9.8 nm and 5.5 nm, respectively, being similar to those of particles prepared through the nucleation at 200 °C (Fig. 2a). These indicated that the size and crystal structure of resulting Cu₂ZnSnS₄ particles were not significantly dependent on the nucleation temperature ranging from 150 to 200 °C.

3.2 Influence of the kind of sulfur precursor on the morphology of Cu₂ZnSnS₄ nanoparticles

It was reported in our previous paper²⁷ that the reaction of corresponding metal acetates with elemental sulfur in pure OLA simply produced spherical Cu₂ZnSnS₄ nanoparticles of a kesterite-type crystal structure at a reaction temperature higher than 240 °C, being different from the present case of using multiple sulfur precursors. Thus, it is thought that the molar ratio of S and DBTU used in a sulfur precursor can affect the size,

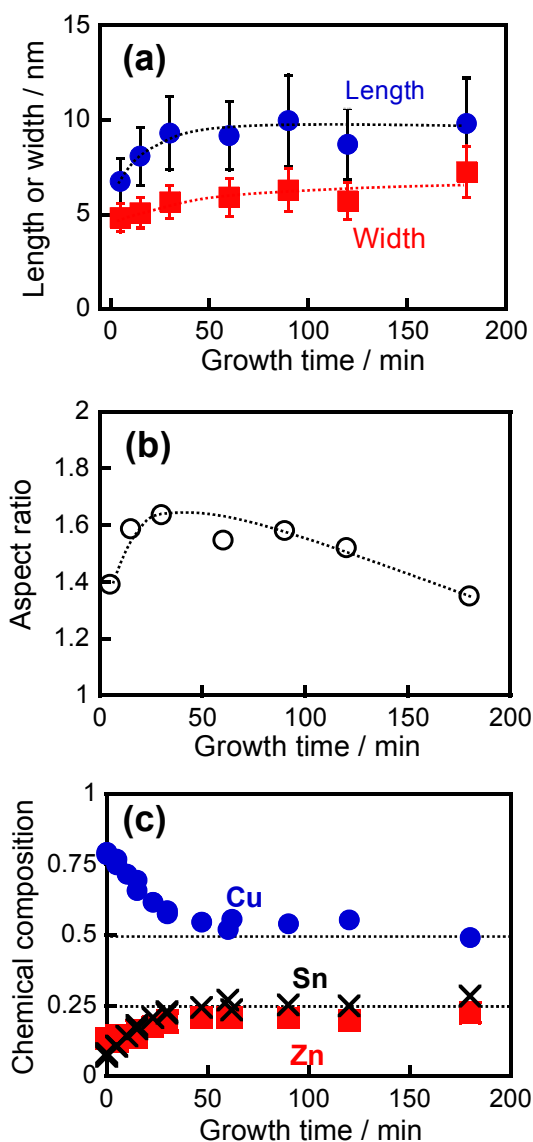


Fig. 4 Change in the morphology (a,b) and chemical composition (c) of nanoparticles with an increase in heating time in the second step. The length (solid circles) and width (solid squares) of particles and their aspect ratio are shown in panels a and b. Error bars in the panel a represent standard deviations of length and width. In panel c, the fractions of metal species are Cu (solid circles), Zn (crosses), and Sn (solid squares).

shape and crystal structure of the resulting $\text{Cu}_2\text{ZnSnS}_4$ particles. Two-step synthesis of $\text{Cu}_2\text{ZnSnS}_4$ particles was carried out by changing the ratio of S to DBTU in a sulfur precursor, in which the total concentration of S and DBTU was fixed at 0.20 mmol. Fig. 3a-e show representative TEM images of nanoparticles prepared with various ratios of S to DBTU. The obtained $\text{Cu}_2\text{ZnSnS}_4$ nanoparticles had a nearly stoichiometric ratio of Cu : Zn : Sn regardless of the precursor ratio of S to DBTU. At a glance, the size and shape of the particles dramatically changed depending on the ratio of S to DBTU: small spherical particles with sizes of ca. 4 nm were formed with injection of pure S, while large wedge- or rod-shaped particles of ca. 50 nm in length and ca. 10 nm in width were produced with the use of pure

DBTU as a sulfur precursor. However, thin rod-shaped particles (width: ca. 4-6 nm) were formed when a mixture of S and DBTU was used. Their length was dependent on the ratio of S to DBTU: the average rod lengths (standard deviations) were determined to 14.3 nm (6.1 nm) for S : DBTU = 75 : 25, 9.3 nm (1.9 nm) for S : DBTU = 50 : 50, and 11.3 nm (4.3 nm) for S : DBTU = 25 : 75, with the precursor ratio of S : DBTU = 50 : 50 being suitable for obtaining wurtzite-type $\text{Cu}_2\text{ZnSnS}_4$ nanoparticles with a narrower size distribution. XRD patterns of these particles shown in Fig. 3f revealed that synthesis in the presence of DBTU produced wurtzite-type $\text{Cu}_2\text{ZnSnS}_4$ nanoparticles, but a pure kesterite phase of $\text{Cu}_2\text{ZnSnS}_4$ nanoparticles appeared only in the case of injection of pure S as a sulfur precursor.

So far, phase-controlled synthesis has usually been performed by changing the kind or ratio of coordinating solvents such as DDT, OLA, ODE, and OAc.^{19,20,22} However, the effect of the coordinating solvent on selective formation of wurtzite-type $\text{Cu}_2\text{ZnSnS}_4$ nanoparticles was not sufficiently discussed in the literature. In the present study, spherical $\text{Cu}_2\text{ZnSnS}_4$ particles with a kesterite structure were formed even in pure DDT by using pure S as a sulfur source, being similar to the synthesis in pure OLA described in our previous paper.²⁷ This suggested that surface modification with DDT was not a key factor to determine the polymorphism of $\text{Cu}_2\text{ZnSnS}_4$ nanocrystals. In contrast, inclusion of DBTU in the sulfur precursor resulted in the production of nanoparticles of wurtzite-type $\text{Cu}_2\text{ZnSnS}_4$ regardless of the fraction of DBTU, indicating that DBTU played an important role in the formation of wurtzite-type $\text{Cu}_2\text{ZnSnS}_4$ nanoparticles. The results showing that pure DBTU only caused the formation of large wedge-like nanoparticles could be reasonably understood by the relatively weak reactivity of DBTU for metal sulfide formation. Active sulfur species would be gradually provided to the solution via thermal decomposition of DBTU, so that a small number of nuclei were generated in the early stage of the reaction along with crystal growth, resulting in the formation of relatively large nanoparticles with a wide size distribution.

3.3 Controlling the crystal growth process

As mentioned in section 3.1, we could assume that the first heating process at 200 °C for 30 min after injection of the sulfur precursor was the "nucleation process" and that the following heating process at 240 °C was the "crystal growth process" of wurtzite $\text{Cu}_2\text{ZnSnS}_4$ nanoparticles. We investigated the reaction time used in the second step to control the degree of crystal growth of wurtzite-type $\text{Cu}_2\text{ZnSnS}_4$ nanocrystals. Synthesis was carried out by injecting the precursor mixture of S and DBTU (50 : 50), with mushroom-like nanoparticles having a heterostructure as shown in Fig. 1a being formed in the first heating process and then used as nuclei for the crystal growth process. With heat treatment at 240 °C for 15 min in the second heating step, the initial mushroom-like particles completely disappeared and then particles with rod or polygon shapes were alternatively formed as shown in Fig. S4b. Prolongation of heat treatment in the second step to 30-180 min resulted in slight changes in the size and shape of the particles (Fig. S4). Fig. 4 shows the changes in morphology of particles and their chemical compositions a function of reaction time used in the second heating step,

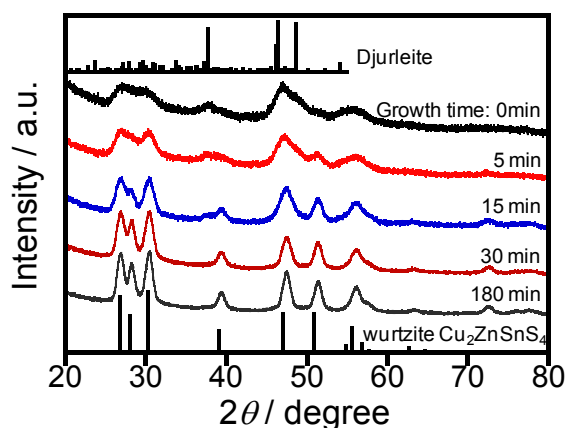


Fig. 5 Change in XRD diffraction pattern of obtained nanoparticles with an increase in reaction time in the second heating step at 240 °C. Reference pattern of djurleite (PDF card: #00-034-0660) and simulated pattern of wurtzite-type $\text{Cu}_2\text{ZnSnS}_4$ shown in ref. 17 are also shown.

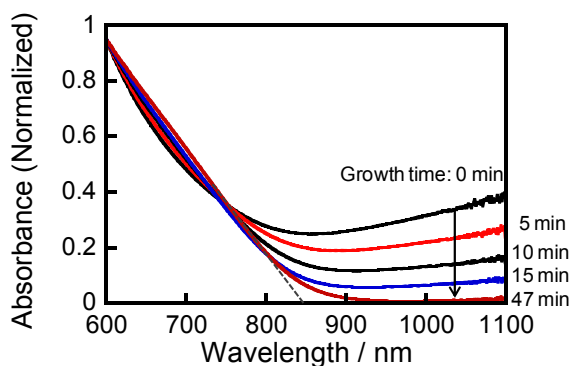


Fig. 6 Change in absorption spectrum of obtained nanoparticles in hexane with an increase in reaction time in the second heating step at 240 °C.

determined from TEM measurement and XRF spectroscopy. In the early stage of crystal growth up to 30 min, the particles anisotropically grew as evidenced by an increase of the aspect ratio from 1.39 to 1.64. By heating for more than 30 min, the width of particles predominantly increased with an increase in the reaction time, but the length was almost constant, resulting in a monotonously decrease of the aspect ratio to ca. 1.4. This suggested an increase in the fraction of polygonal particles with nearly isotropic shapes along with crystal growth. Cu-rich nanoparticles with the composition of Cu : Zn : Sn = 0.79 : 0.13 : 0.08 were formed just after the nucleation process. With elapse of heating time in the crystal growth process, Zn and Sn ions were gradually incorporated into the nanoparticles. A nearly stoichiometric composition of $\text{Cu}_2\text{ZnSnS}_4$ particles was obtained by heating for more than 30 min. These results suggested that the incorporation of Sn and Zn ions dissolved in the solution into nanocrystals induced elongation of $\text{Cu}_2\text{ZnSnS}_4$ rod particles in which the aspect ratio increased from 1.39 to 1.64.

Fig. 5 shows changes in the XRD patterns of particles obtained with different reaction times. As aforementioned, the nuclei, that

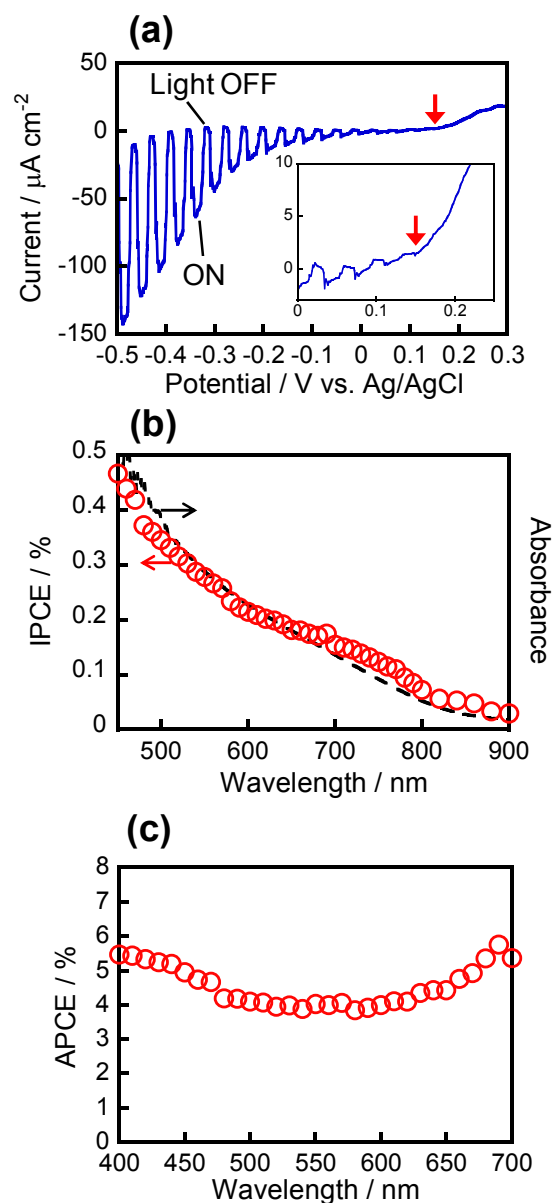
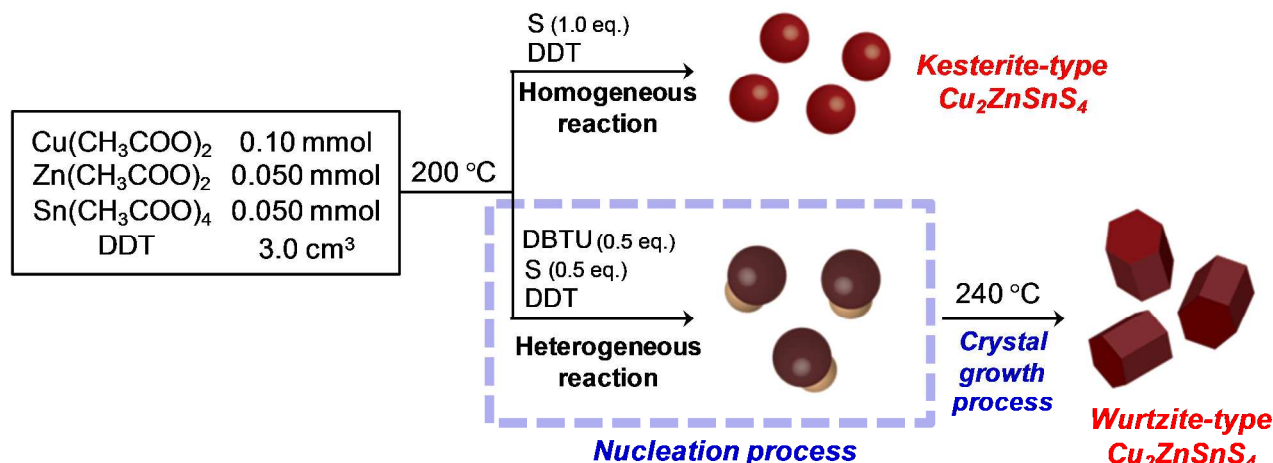


Fig. 7 (a) Photocurrent-potential curves of wurtzite-type $\text{Cu}_2\text{ZnSnS}_4$ nanoparticles immobilized on an ITO electrode. An arrow shows the onset potential of the photocurrent. (b) IPCE and (c) APCE of the wurtzite-type $\text{Cu}_2\text{ZnSnS}_4$ nanoparticulate electrode measured under potential application of -0.5 V vs. Ag/AgCl. Broken line in panel b represents absorption spectrum of the corresponding wurtzite-type $\text{Cu}_2\text{ZnSnS}_4$ nanoparticles in hexane.

is, particles heat-treated in the second heating process for 0 min, contained two crystal phases consisting of a djurleite $\text{Cu}_{1.94}\text{S}$ crystal exhibiting a strong diffraction peak at ca. 38° and a wurtzite $\text{Cu}_2\text{ZnSnS}_4$ crystal exhibiting peaks at around 27, 28, 30, 39, 47, 51, and 56°. With an increase in reaction time, the peaks assignable to wurtzite $\text{Cu}_2\text{ZnSnS}_4$ crystal became sharper, but the intensity of a broad peak at 38° assigned to djurleite $\text{Cu}_{1.94}\text{S}$ crystal decreased. Particles heat-treated for more than 30 min exhibited diffraction peaks assignable to only wurtzite structure. This behavior was in good agreement with the change in chemical composition of particles with the crystal growth process



Scheme 1 Schematic diagram of the synthesis of kesterite- and wurtzite-type $\text{Cu}_2\text{ZnSnS}_4$ nanoparticles.

as shown in Fig. 4c: a nearly stoichiometric composition of $\text{Cu}_2\text{ZnSnS}_4$ particles was obtained by heating for more than 30 min, while Cu-rich nanoparticles were formed at the initial stage of reaction.

The absorption spectra of particles dispersed in the solution support the disappearance of djurleite along with formation of stoichiometric $\text{Cu}_2\text{ZnSnS}_4$ having a wurtzite phase. As shown in Fig. 6, a broad absorption band was observed in the near-IR region with a wavelength longer than 900 nm in the case of particles just after the nucleation process, which was assigned to localized surface plasmon resonance (LSPR) absorption of djurleite nanoparticles of $\text{Cu}_{1.94}\text{S}$.^{25,28} This LSPR-peak intensity of $\text{Cu}_{1.94}\text{S}$ decreased with elapse of reaction time and finally the absorption onset appeared at ca. 850 nm, roughly corresponding to the energy gap of wurtzite-type $\text{Cu}_2\text{ZnSnS}_4$ (~1.5 eV).¹⁸⁻²¹

3.4 Mechanism of crystal-phase-selective formation of $\text{Cu}_2\text{ZnSnS}_4$ nanoparticles

We successfully developed crystal-phase-selective synthesis of $\text{Cu}_2\text{ZnSnS}_4$ nanoparticles, in which the crystal structure of $\text{Cu}_2\text{ZnSnS}_4$ nanoparticles, wurtzite- or kesterite-type, could be controlled only by changing the molar ratio of the two different sulfur sources. The results obtained in this study are summarized in Scheme 1. For the formation of wurtzite-type $\text{Cu}_2\text{ZnSnS}_4$ nanoparticles, an equal molar ratio of S and DBTU (S : DBTU = 50 : 50) produced mushroom-like nuclei (Fig. 1a). Similar heterostructured nanoparticles have been reported for multinary metal chalcogenide semiconductors. For example, Gao *et al.* reported tadpole-like nanoparticles composed of djurleite $\text{Cu}_{1.94}\text{S}$ as the "head" and wurtzite-type ZnS as the "tail",²⁹ in which the wurtzite-type ZnS epitaxially grew on monoclinic $\text{Cu}_{1.94}\text{S}$ along the *c*-crystallographic axis. The anisotropic growth of wurtzite ZnS was derived from the small lattice mismatch on the corresponding interface of djurleite $\text{Cu}_{1.94}\text{S}$.^{29,30} The formation of heterostructured nuclei shown in Fig. 1a can be explained by a similar mechanism.

We propose the following mechanism for the selective formation of wurtzite-type $\text{Cu}_2\text{ZnSnS}_4$ particles. At first, during the heating at 200 °C as the nucleation process, djurleite $\text{Cu}_{1.94}\text{S}$ nanoparticles were formed by the reaction of Cu precursors with a more reactive precursor of S (0.5 eq. to the metal precursors) because Cu sulfide is apt to form more easily than those of Zn and Sn.²³ Along with the formation of djurleite nuclei, thermal decomposition of DBTU gradually occurred to release additional active sulfur species, resulting in the formation of a wurtzite-type ZnS (or Cu- and Sn-doped ZnS) crystal phase that was anisotropically grown from thus-obtained djurleite $\text{Cu}_{1.94}\text{S}$ nanoparticles. In the following heating step at a higher temperature of 240 °C as the second step, the ions remaining in the solution, such as Zn and Sn, reacted with an active sulfur species that was formed by the complete decomposition of DBTU or metal thiolates partially decomposed to form metal sulfides, resulting in crystal growth of the nuclei.

Heat treatment at a temperature higher than 240 °C was essential in the present study for the formation of stoichiometric wurtzite-type $\text{Cu}_2\text{ZnSnS}_4$ nanoparticles. It has been reported that the formation of homogeneous nanoparticles was based on crystal growth accompanied by interdiffusion of Cu ions in the nanoparticles at a higher temperature.¹⁹⁻²¹ In addition, a ripening process via forward and backward reactions in the system should also relate to the formation of the homogeneous nanoparticles. The forward reactions consisted of the formation of metal sulfides by reaction of metal thiolates with injected sulfur precursors and by partial decomposition of metal thiolates, while the backward reaction was dissolution of metal sulfide nanoparticles by DDT to regenerate metal thiolates. When the reaction temperature was raised to 240 °C, the forward and backward reactions should repeatedly occur until the reaction reaches an apparent equilibrium in the system, resulting in formation of wurtzite-type $\text{Cu}_2\text{ZnSnS}_4$ nanoparticles with a stable shape and chemical composition. So far, it has been reported that pure wurtzite-type $\text{Cu}_2\text{ZnSnS}_4$ nanoparticles were synthesized only at high temperature (> 210 °C) in the presence of

alkylthiol.¹⁷⁻²⁴ These can support the mechanism described above.

On the other hand, kesterite-type $\text{Cu}_2\text{ZnSnS}_4$ particles could be selectively formed only in the case of the metal precursors having completely reacted with a sulfur source to form metal sulfides in a single step. For example, when a 0.20 mmol portion of S (1.0 eq. to the metal precursors) was injected into the reaction solution, the total amounts of metal precursors homogeneously reacted due to the addition of a sufficient amount of a highly reactive sulfur source, resulting in thermodynamically stable $\text{Cu}_2\text{ZnSnS}_4$ nanoparticles of a kesterite structure without formation of djurleite $\text{Cu}_{1.94}\text{S}$ nuclei.

3.5 Photoelectrochemical properties of wurtzite-type $\text{Cu}_2\text{ZnSnS}_4$ nanoparticles depending on the crystal structure.

Photoelectrochemical measurements were carried out in order to evaluate photoelectrochemical properties of wurtzite-type $\text{Cu}_2\text{ZnSnS}_4$ nanoparticles, in comparison with kesterite-type $\text{Cu}_2\text{ZnSnS}_4$ nanoparticles. Fig. 7a shows a photocurrent-potential curve of a $\text{Cu}_2\text{ZnSnS}_4$ nanoparticle-immobilized electrode measured in an $\text{Eu}(\text{NO}_3)_3$ aqueous solution upon intermittent light irradiation ($\lambda > 350$ nm), where wurtzite-type particles of 9.3 nm in length and 5.7 nm in width as shown in Fig. 2a were used. A cathodic photocurrent was observed with light irradiation, indicating that the wurtzite-type $\text{Cu}_2\text{ZnSnS}_4$ nanoparticles behaved as a p -type semiconductor, being similar to kesterite-type ones. In the case of bulk p -type semiconductor electrodes, photogenerated holes diffuse inside the semiconductor and then can be injected into a contacting electrode as long as the electrode potential is more negative than that of the flatband potential (E_{FB}). Therefore, it is reasonably assumed that E_{FB} in most p -type semiconductors is comparable to the potential of the valence band edge (E_{VB}). The onset potential of the cathodic photocurrent in Fig. 7a could be regarded as E_{VB} and was determined to be ca. +0.15 V vs. Ag/AgCl, the value of which agreed with that previously reported for kesterite-type $\text{Cu}_2\text{ZnSnS}_4$ nanoparticles of 5-6 nm in diameter.^{15,27}

The action spectrum of the cathodic photocurrent is shown in Fig. 7b. The onset wavelength appeared at ca. 850-900 nm, being in rough agreement with the absorption onset of particles in the solution. Since the prepared film was very thin with absorbance of ca. 0.08 at 400 nm to avoid carrier trapping inside the particulate films, the obtained IPCE was relatively low (< ca. 0.6 %). The absorbed photon-to-current efficiency (APCE), calculated by dividing the number of electrons detected in the photocurrent by that of photons absorbed by $\text{Cu}_2\text{ZnSnS}_4$ film, was ca. 4-5% as shown in Fig. 7c, regardless of the wavelength of irradiating monochromatic light. It should be noted that the present wurtzite-type $\text{Cu}_2\text{ZnSnS}_4$ nanoparticles exhibited a ca. 10-times larger IPCE value than those obtained with kesterite-type ones: as reported in our previous paper,¹⁶ the photoelectrochemical activity of ITO electrodes modified with kesterite-type $\text{Cu}_2\text{ZnSnS}_4$ particles, the absorbance of which was ca. 0.045 at 400 nm, was considerably dependent on the chemical composition, and the maximum IPCE value at 400 nm irradiation was 0.045% (corresponding to APCE of 0.48%) with the use of particles having the composition of Cu : Zn : Sn = 0.47 : 0.23 : 0.29. These results suggest that wurtzite-type $\text{Cu}_2\text{ZnSnS}_4$

nanoparticles showed better performance than kesterite-type ones as a photovoltaic material. This is consistent with the results of a previous study showing that wurtzite-type $\text{Cu}_2\text{ZnSnS}_4$ nanoparticles had a higher carrier concentration and lower resistivity than those of kesterite-type ones.¹⁹

Conclusions

We demonstrated well-defined synthesis of wurtzite-type $\text{Cu}_2\text{ZnSnS}_4$ nanoparticles using two different sulfur sources via a two-step heating process. The method could clearly distinguish a nucleation process from a crystal growth process. In the nucleation process, injection of the sulfur precursor mixture, S and DBTU (with 50 : 50 ratio), into the metal precursor solution enabled the formation of heterostructured particles composed of wurtzite-type $\text{Cu}_2\text{ZnSnS}_4$ and djurleite $\text{Cu}_{1.94}\text{S}$ nanoparticles. In the following crystal growth process, these particles acted as nuclei to produce wurtzite-type $\text{Cu}_2\text{ZnSnS}_4$ nanoparticles with a stoichiometric composition. In addition, the morphology of particles, chemical composition, and crystal structure could be controlled by changing the reaction conditions, including the molar ratio of S and DBTU, reaction temperature, and reaction time. This well-controlled method for synthesis of wurtzite-type $\text{Cu}_2\text{ZnSnS}_4$ nanoparticles will have a great impact on studies not only on $\text{Cu}_2\text{ZnSnS}_4$ nanoparticles but also on other multinary metal sulfide semiconductor nanoparticles such as CuInS_2 because they can also form a meta-stable wurtzite-type structure from copper sulfide nuclei.³²

Another interesting finding is that the photoelectrochemical properties of $\text{Cu}_2\text{ZnSnS}_4$ nanoparticles varied depending on the kind of crystal structure. Notably, the light-electricity conversion efficiency of wurtzite-type particles was much higher than that of kesterite-type ones, suggesting prominent properties of the wurtzite-type nanoparticles as an efficient light-absorbing material for photovoltaic applications. Improvement in the method for synthesis of wurtzite-type $\text{Cu}_2\text{ZnSnS}_4$ nanoparticles should increase the light energy conversion efficiency and lead to the development of novel low-cost and highly efficient light energy conversion systems.

Acknowledgements

This work was supported by a Funding Program for Next Generation World-Leading Researchers (NEXT Program) and a Grant-in-Aid of for Young Scientists (B) (No. 26810043) from the Japan Society for the Promotion of Science.

Notes and references

^a Department of Crystalline Materials Science, Graduate School of Engineering, Nagoya University, Furo-cho, Chikusa-ku, Nagoya 464-8603, Japan.

^b Department of Applied Chemistry, Graduate School of Engineering, Osaka University, 2-1 Yamada-oka, Suita, Osaka 565-0871, Japan.

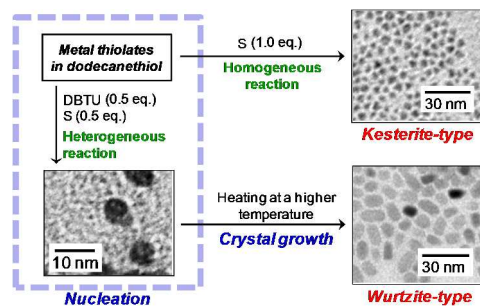
† Electronic Supplementary Information (ESI) available: TEM image of nanoparticles produced by thermal decomposition of metal thiolates in DDT at 240 °C for 60 min (Fig. S1); TEM image and XRD pattern of nanoparticles prepared by addition of an equal molar ratio of S and DBTU and subsequent stirring at 200 °C for 180 min (Fig. S2); TEM image and XRD pattern of nanoparticles prepared through the nucleation process at 150 °C for 30 min (Fig. S3). TEM images of nanoparticles obtained after

the crystal growth process for 0-180 min (Fig. S4). See DOI: 10.1039/b000000x/

‡ Present address: Institute of Industrial Science, The University of Tokyo, 4-6-1 Komaba, Meguro-ku, Tokyo 153-8505, Japan. E-mail: nishi-h@iis.u-tokyo.ac.jp

- 1 K. Ramasamy, M. A. Malik, P. O'Brien, *Chem. Commun.*, 2012, **48**, 5703-5714.
- 2 S. Delbos, *EPJ Photovoltaics*, 2012, **3**, 35004.
- 10 3 W. Wang, M. T. Winkler, O. Gunawan, T. Gokmen, T. K. Todorov, Y. Zhu, D. B. Mitzi, *Adv. Energy Mater.*, 2014, **4**, 1301465.
- 4 D. A. R. Barkhouse, O. Gunawan, T. Gokmen, T. K. Todorov, D. B. Mitzi, *Prog. Photovolt: Res. Appl.*, 2012, **20**, 6-11.
- 5 K. Wang, O. Gunawan, T. Todorov, B. Shin, S. J. Chey, N. A. Bojarczuk, D. Mitzi, S. Guha, *Appl. Phys. Lett.*, 2010, **97**, 143508.
- 15 6 G. Khrypunov, A. Remeo, F. Kurdeasu, D. L. Bätzner, H. Zogg, A. N. Tiwari, *Sol. Eng. Mat. Sol. C.*, 2006, **90**, 664-677.
- 7 M. Law, J. M. Luther, Q. S. Barbara, K. Hughes, C. L. Perkins, A. J. Nozik, *J. Am. Chem. Soc.*, 2008, **130**, 5974-5985.
- 20 8 P. Jackson, D. Hariskos, E. Lotter, S. Paetel, R. Wuerz, R. Menner, W. Wischmann, M. Powalla, *Prog. Photovolt: Res. Appl.*, 2011, **19**, 894-897.
- 9 I. Repins, M. A. Contreras, B. Egaas, C. DeHart, J. Scharf, C. L. Perkins, B. To, R. Noufi, *Prog. Photovolt: Res. Appl.*, 2008, **16**, 235-239.
- 25 10 Q. Guo, H. W. Hillhouse, R. Agrawal, *J. Am. Chem. Soc.*, 2009, **131**, 11672-11673.
- 11 Q. Guo, G. M. Ford, W.-C. Yang, B. C. Walker, E. A. Stach, H. W. Hillhouse, R. Agrawal, *J. Am. Chem. Soc.*, 2010, **132**, 17384-17386.
- 30 12 A. Khare, A. W. Wills, L. M. Ammerman, D. J. Norris, E. S. Aydil, *Chem. Commun.*, 2011, **47**, 11721-11723.
- 13 W. C. Liu, B. L. Guo, X. S. Wu, F. M. Zhang, C. L. Mak, K. H. Wong, *J. Mater. Chem. A*, 2013, **1**, 3182-3186.
- 14 A. J. Nozik, M. C. Beard, J. M. Luther, M. Law, R. J. Ellingson, J. C. Johnson, *Chem. Rev.*, 2010, **110**, 6873-6890.
- 35 15 H. Nishi, T. Nagano, S. Kuwabata, T. Torimoto, *Phys. Chem. Chem. Phys.*, 2014, **16**, 672-675.
- 16 H. Nishi, S. Kuwabata, T. Torimoto, *J. Phys. Chem. C*, 2013, **117**, 21055-21063.
- 40 17 X. Lu, Z. Zhuang, Q. Peng, Y. Li, *Chem. Commun.*, 2011, **47**, 3141-3143.
- 18 A. Singh, H. Geaney, F. Laffir, K. M. Ryan, *J. Am. Chem. Soc.*, 2012, **134**, 2910-2913.
- 19 M. Li, W.-H. Zhou, J. Guo, Y.-L. Zhou, Z.-L. Hou, J. Jiao, Z.-J. Zhou, Z.-L. Du, S.-X. Wu, *J. Phys. Chem. C*, 2012, **116**, 26507-26516.
- 45 20 M.-D. Regulacio, C. Ye, S. H. Lim, M. Bosman, E. Ye, S. Chen, Q.-H. Xu, M.-Y. Han, *Chem. Eur. J.*, 2012, **18**, 3127-3131.
- 21 H.-C. Liao, M.-H. Jao, J.-J. Shyue, Y.-F. Chen, W.-F. Su, *J. Mater. Chem. A*, 2013, **1**, 337-341.
- 50 22 J. Chang, E. R. Waclawik, *CrystEngComm*, 2013, **15**, 5612-5619.
- 23 M. J. Thompson, T. P. A. Ruberu, K. J. Blakeney, K. V. Torres, P. S. Dilsaver, J. Vela, *J. Phys. Chem. Lett.*, 2013, **4**, 3918-3923.
- 24 Y. Zou, X. Su, J. Jiang, *J. Am. Chem. Soc.*, 2013, **135**, 18377-18384.
- 55 25 M. Kanehara, H. Arakawa, T. Honda, M. Saruyama, T. Teranishi, *Chem. Eur. J.*, 2012, **18**, 9230-9238.
- 26 D. Mott, J. Yin, M. Engelhard, R. Loukrakpam, P. Chang, G. Miller, I.-T. Bae, N. C. Das, C. Wang, J. Luo, C.-J. Zhong, *Chem. Mater.*, 2010, **1**, 261-271.
- 60 27 T. Kameyama, T. Osaki, K. Okazaki, T. Shibayama, A. Kudo, S. Kuwabata, T. Torimoto, *J. Mater. Chem.*, 2010, **20**, 5319-5324.
- 28 J. M. Luther, P. K. Jain, T. Ewers, A. P. Alivisatos, *Nature Mater.*, 2011, **10**, 361-366.
- 29 L. Yi, A. Tang, M. Niu, W. Han, Y. Hou, M. Gao, *CrystEngComm*, 2010, **12**, 4124-4130.
- 65 30 S.-K. Han, M. Gong, H.-B. Yao, Z.-M. Wang, S.-H. Yu, *Angew. Chem. Int. Ed.*, 2012, **51**, 6365-6368.
- 31 D. A. R. Barkhouse, A. G. Pattantyus-Abraham, L. Levina, E. H. Sargent, *ACS Nano*, 2008, **2**, 2356-2362.
- 70 32 M. Kruszynska, H. Borchert, J. Parisi, J. Kolny-Olesiak, *J. Am. Chem. Soc.*, 2010, **132**, 15976-15986.

TOC graphic



Wurtzite-type $\text{Cu}_2\text{ZnSnS}_4$ nanoparticles were successfully synthesized by a new approach that could control morphology, chemical composition, and crystal structure of the particles. Formation mechanism was discussed in detail.